Few-cycle pulse propagation

P. Kinsler* and G. H. C. New
Department of Physics, Imperial College, Prince Consort Road, London SW7 2BW, United Kingdom
(Received 12 September 2002; published 28 February 2003)

We present a comprehensive framework for treating the nonlinear interaction of few-cycle pulses using an envelope description that goes beyond the traditional slowly varying envelope approximation method. This is applied to a range of simulations that demonstrate how the effect of a $\chi^{(2)}$ nonlinearity differs between the many-cycle and few-cycle cases. Our approach, which includes diffraction, dispersion, multiple fields, and a wide range of nonlinearities, builds upon the work of Brabec and Krausz [T. Brabec and F. Krausz, Phys. Rev. Lett. **78**, 3282 (1997)] and Porras [M. A. Porras, Phys. Rev. A **60**, 5069 (1999)]. No approximations are made until the final stage when a particular problem is considered.

DOI: 10.1103/PhysRevA.67.023813 PACS number(s): 42.65.Re,42.65.Yj

I. INTRODUCTION

The analysis of optical pulse propagation traditionally involves describing a pulse in terms of a complex field envelope, while neglecting the underlying rapid oscillations at its carrier frequency. The resulting ''slowly varying envelope approximation'' (SVEA) (see e.g., Ref. [3]), which reduces second-order differential equations to first order, is valid when the envelope encompasses many cycles of the optical field and varies slowly. The alternative approach is to solve Maxwell's equations numerically (see e.g., Refs. [1,4]), which is more general but involves greater computational effort, and lacks the intuitive picture of a pulse ''envelope.''

For example, optical parametric oscillators (OPOs) based on aperiodically poled lithium niobate have generated 53-fs idler pulses at 3 μm that are nearly transform limited, and contain only five optical cycles [5]; laser pulses with less than three optical cycles have been generated in other contexts [6]. Under these circumstances, the validity of the slowly varying envelope approximation is clearly open to question.

Brabec and Krausz [1] derived corrections to the SVEA, which they included in their ''slowly evolving wave approximation'' (SEWA). This enabled the few-cycle regime to be modeled with improved accuracy, and the SEWA has subsequently been applied in different situations, including ultrashort IR laser pulses in fused silica [7,8], the filamentation of ultrashort laser pulses in air [9], and even in microstructured optical fibres [10]. Later, Porras [2] proposed a slightly different ''slowly evolving envelope approximation'' (SEEA) that included corrections for the transverse behavior of the field.

Here we use a field envelope approach to simulate the propagation of ultrashort pulses in a $\chi^{(2)}$ medium. The difference is that we (a) derive a more general form than that of Brabec and Krausz, called the ''generalized few-cycle envelope approximation''(GFEA); and (b) apply it to both optical (nondegenerate) parametric amplification (NPA) and the optical parametric oscillator (OPO). More comprehensive results, including some for a variety of systems such as second harmonic generation and degenerate parametric amplification, can be seen in Ref. [11]. The only previous multiple field application of this kind of result was for four wave mixing [12].

We compare the SEWA-SEEA equations to our own (Sec. II), and explain the differences and subsequent adjustments to the necessary approximations. This theory enables us to rigorously study what combination of approximations affords the most efficient method for treating a given nonlinear interaction involving few-cycle pulses. Next (Sec. III) we discuss the $\chi^{(2)}$ nonlinearity and a scaling scheme designed to reveal the few-cycle effects. Then we compare the SVEA predictions to the few-cycle GFEA theory using idealized situations (Sec. IV) and more realistic OPO models (Sec. V). Finally, we present our conclusions (Sec. VI).

II. THEORY

This section contains a summary of a complete rederivation [13] of a Brabec and Krausz style theory, which yields an evolution equation for an envelope description of pulse propagation in the few-cycle regime. Our result is more complicated than the SEWA equation [1], but reduces to it in the appropriate limits; it also explains the slight differences between their result and that of Porras [2].

Following Brabec-Krausz, we consider the case of small transverse inhomogeneities of the polarization, and so start with the three-dimensional wave equation

$$(\partial_z^2+\nabla_\perp^2)E(\vec{r},t)-\frac{1}{c^2}\partial_t^2\int_{-\infty}^{t}dt'\,\epsilon(t-t')E(\vec{r},t')$$

$$=\frac{4\pi}{c^2}\partial_t^2 P_{nl}(\vec{r},t). \tag{1}$$

Here $\nabla_\perp^2$ is the transverse Laplace operator, ∂_α is shorthand notation for $\partial/\partial\alpha$, $\epsilon(t)=(2\pi)^{-1}\int_{-\infty}^{\infty}d\omega\tilde{\epsilon}(\omega)e^{\imath\omega t}$, $\tilde{\epsilon}(\omega)=1+4\pi\chi(\omega)$, and $\chi(\omega)$ is the linear electric susceptibility. The electric field E propagates along the z direction. Both E and the nonlinear polarization P_{nl} are polarized parallel to the x axis.

*Electronic address: Dr.Paul.Kinsler@physics.org

We can transform Eq. (1) into frequency space in order to expand $\tilde{\epsilon}(\omega)$ in powers of ω, thus enabling us to treat the material parameters as a power series which we can truncate to an appropriate order. However, for simplicity it is better to expand k about a suitable ω_0 instead. Using $\tilde{\epsilon}(\omega) = c^2 k(\omega)^2/\omega^2$, it follows that

$$k(\omega) = \sum_{n=0}^{\infty} \frac{\gamma_n (\omega-\omega_0)^n}{n!},$$

$$\gamma_n = \partial_\omega^n k(\omega)\big|_{\omega_0} = \beta_n + \imath\alpha_n ; \beta_n, \alpha_n \in \mathbb{R}. \tag{2}$$

We can now write the frequency space version of Eq. (1) as

$$(\partial_z^2 + \nabla_\perp^2) E(\vec{r},t) + \left[\sum_{n=0}^{\infty} \frac{\imath^n \gamma_n (\partial_t + \imath\omega_0)^n}{n!}\right]^2 E(\vec{r},t) = \frac{4\pi}{c^2}\partial_t^2 P_{nl}(\vec{r},t). \tag{3}$$

We introduce an envelope and carrier form for the field in the usual way, using $\vec{r} \equiv (\vec{r}_\perp, z)$, so that

$$E(\vec{r},t) = A(\vec{r}_\perp,z,t)e^{\imath\Xi} + A^*(\vec{r}_\perp,z,t)e^{-\imath\Xi}, \tag{4}$$

and similarly $P_{nl}(\vec{r},t) = B(\vec{r}_\perp,z,t;A)e^{\imath\Xi} + B^*(\vec{r}_\perp,z,t;A)e^{-\imath\Xi}$. The symbol $\Xi = \beta_0 z - \omega_0 t + \psi_0$ is introduced as a convenient shorthand for the argument of the exponential. With these envelope-carrier substitutions, the equation of motion can be written as

$$([\imath\beta_0 + \partial_z]^2 + \nabla_\perp^2) A(\vec{r}_\perp,z,t) + \left[\sum_{n=0}^{\infty} \frac{\gamma_n \omega_0^n}{n!}\left(\frac{\imath}{\omega_0}\partial_t\right)^n\right]^2 A(\vec{r}_\perp,z,t) = -\frac{4\pi\omega_0^2}{c^2}\left(1 + \frac{\imath}{\omega_0}\partial_t\right)^2 B(\vec{r}_\perp,z,t;A). \tag{5}$$

Equation (5) has the opposite sign on the RHS to Brabec and Krausz's Equation (2), but agreement is recovered later in Eq. (11).

As usual, we introduce comoving variables

$$\tau = \omega_0(t - \beta_1 z), \quad \partial_t \equiv \omega_0 \partial_\tau, \tag{6}$$

$$\xi = \beta_0 z, \quad \partial_z \equiv \beta_0 \partial_\xi - \omega_0\beta_1\partial_\tau, \tag{7}$$

and Eq. (5) now becomes

$$\left\{(\imath\beta_0 + \beta_0\partial_\xi - \omega_0\beta_1\partial_\tau)^2 + \nabla_\perp^2 + \left[\sum_{n=0}^{\infty} \frac{\gamma_n\omega_0^n}{n!}(\imath\partial_\tau)^n\right]^2\right\} A(\vec{r}_\perp,\xi,\tau) + \frac{4\pi\omega_0^2}{c^2} \times (1+\imath\partial_\tau)^2 B(\vec{r}_\perp,\xi,\tau;A) = 0. \tag{8}$$

For convenience we also introduce the dimensionless ratio of phase and group velocities $\sigma = \omega_0\beta_1/\beta_0 = (\omega_0/\beta_0)/(1/\beta_1) = v_f/v_g$, and use the fact that the refractive index at ω_0 is $n_0 = c\beta_0/\omega_0$. We also define a dispersion term $\hat{D}$ in a similar way to Brabec-Krausz, but instead use a scaled (dimensionless) version $\hat{D}' = (\omega_0/\beta_0)\hat{D}$ in the following equations so that

$$\hat{D}' = \frac{\omega_0}{\beta_0}\left[\imath\alpha_1(\imath\partial_\tau) + \sum_{n=2}^{\infty} \frac{\gamma_n\omega_0^{n-1}}{n!}(\imath\partial_\tau)^n\right]. \tag{9}$$

Hence we get

$$0 = \left\{(\partial_\xi - \sigma\partial_\tau) + \frac{1}{2\imath}(\partial_\xi - \sigma\partial_\tau)^2 + \frac{1}{2\imath\beta_0^2}\nabla_\perp^2 - \left[\imath\sigma(\imath\partial_\tau) - \frac{\imath\alpha_0}{\beta_0} + \imath\hat{D}'\right] + \frac{\imath}{2}\left[\imath\sigma(\imath\partial_\tau) - \frac{\imath\alpha_0}{\beta_0} + \imath\hat{D}'\right]^2\right\} A(\vec{r}_\perp,\xi,\tau) + \frac{2\pi}{\imath n_0^2}(1+\imath\partial_\tau)^2 B(\vec{r}_\perp,\xi,\tau;A). \tag{10}$$

This form can be rearranged without approximation to

$$\partial_\xi A(\vec{r}_\perp,\xi,\tau) = \left(-\frac{\alpha_0}{\beta_0} + \imath\hat{D}'\right) A(\vec{r}_\perp,\xi,\tau) + \frac{(\imath/2\beta_0^2)\nabla_\perp^2}{(1+\imath\sigma\partial_\tau)} A(\vec{r}_\perp,\xi,\tau) + \frac{2\imath\pi}{n_0^2}\frac{(1+\imath\partial_\tau)^2}{(1+\imath\sigma\partial_\tau)} B(\vec{r}_\perp,\xi,\tau;A) + \frac{T_R}{1+\imath\sigma\partial_\tau}, \tag{11}$$

where

$$T_R = \left[-\frac{\imath q^2}{2}\partial_\xi^2 + \frac{\imath}{2}\left(\frac{\alpha_0}{\beta_0} - \imath\hat{D}'\right)^2\right] A(\vec{r}_\perp,\xi,\tau). \tag{12}$$

Equation (11) *is exact*—it contains no more approximations than our starting point Eq. (1) except for the expansion of ϵ in powers of ω. We recover the full field E from Eq. (4) by recombining A and knowing the carrier. The partial derivatives $(\imath\partial_\tau)$ in the denominators can, if necessary, be treated by Fourier transforming into the conjugate frequency space (Ω). Note that like τ, Ω is scaled relative to the carrier frequency.

If we set $T_R=0$, this gives us a GFEA equation, which contains the SVEA [3], SEWA [1], and SEEA [2] within it as special cases. Of course we cannot just set the T_R term to zero without some justification, and this is discussed below.

The $(2\imath\pi/n_0^2)\mathcal{K}B$ polarization term from Eq. (11) has prefactors that depend on the time derivative of the polarization, and these new terms are what add the effect of finite pulse lengths to the pulse evolution. Note that we can write this polarization term in different forms,

$$\mathcal{K}=\frac{(1+\imath\partial_\tau)^2}{(1+\imath\sigma\partial_\tau)}=(1+\imath\sigma\partial_\tau)\left[1+(1-\sigma)\frac{2\imath\partial_\tau+(1+\sigma)\partial_\tau^2}{(1+\imath\sigma\partial_\tau)^2}\right]$$

$$=(1+\imath\partial_\tau)\left[1+\frac{\imath(1-\sigma)\partial_\tau}{(1+\imath\sigma\partial_\tau)^2}\right]. \tag{13}$$

With $\sigma=1$, these reduce to the $\mathcal{K}=1+\imath\partial_\tau$ SEWA [1] form. Similarly, to first order in $(\sigma-1)$, one can get the $\mathcal{K}=1+\imath\sigma\partial_\tau$ SEEA [2] form. Finally, for a SVEA theory, $\mathcal{K}=1$, since the ∂_τ terms are assumed to be negligible.

The T_R term is negligible if the following conditions hold: (i) Dispersion terms in ∂_τ can be neglected if

$$\left|\left(\frac{\omega_0^m\gamma_m'}{\beta_0 m!}\Omega^m\right)\tilde{A}(\vec{r}_\perp,\xi,\Omega)\right|\ll|\tilde{A}(\vec{r}_\perp,\xi,\Omega)|. \tag{14}$$

(ii) Evolution terms in ∂_ξ^2 can be neglected if

$$|\partial_\xi\tilde{A}(\vec{r}_\perp,\xi,\Omega)|\ll|\tilde{A}(\vec{r}_\perp,\xi,\Omega)|, \tag{15}$$

and Eq. (15) only holds if, in addition, (iii) diffraction terms in $\nabla_\perp^2$ can be neglected if

$$(1+\sigma\Omega)\beta_0^2w_0^2\gg1, \tag{16}$$

(iv) nonlinearity is "weak" if

$$\frac{n_0^2}{2\pi}\frac{(1+\sigma\Omega)}{(1+\Omega)^2}\gg\frac{|\tilde{B}(\vec{r}_\perp,\xi,\Omega;A)|}{|\tilde{A}(\vec{r}_\perp,\xi,\Omega)|}. \tag{17}$$

We use Ω instead of $\imath\partial_\tau$ for these conditions because conditions, on the frequency components of the various terms are better defined than those for time derivatives.

These conditions are the same as those required for the SEWA and SEEA theories, with the SVEA conditions being a special case gained by setting $|\Omega|\ll1$ for the diffraction and nonlinearity conditions—implying that modulations in the envelope are so slow compared to the carrier frequency that they can be neglected. Note that backward propagating behavior has not been explicitly excluded, but since it would appear as a modulation on the envelope A, it would be approximated away as part of the evolution condition [Eq. (15)].

Note that the exact solution of Eq. (11) makes no reference to a particular choice of carrier phase ψ_0. This implies that once a solution for the propagation of a particular envelope has been obtained, the problem has, in fact, been solved for a set of pulses (and initial conditions) based on different carrier phases—where that set is determined by the initial envelope and some arbitrary choices of carrier phase $\psi_1\in[0,2\pi)$. The final state is then given by the chosen ψ_1 combined with the final form of the envelope.

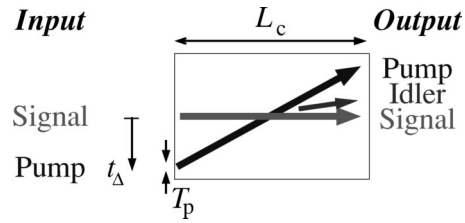

FIG. 1. Pump timing offset (see Sec. III). The pump pulse is injected into the crystal just before the signal pulse is reflected off the input mirror. The faster moving signal pulse then catches the pump pulse up about halfway through the crystal, and an idler pulse is generated.

III. THE $\chi^{(2)}$ NONLINEAR SYSTEM

When modeling $\chi^{(2)}$ nonlinear systems we split the optical field into two or three parts, depending on whether a degenerate or nondegenerate system is being treated. For example, a parametric amplifier would have pump, signal, and idler field components. We then define an envelope A_α and carrier $e^{\imath\Xi_\alpha}$, $\Xi_\alpha=\beta_{\alpha,0}z-\omega_{\alpha,0}t+\psi_{\alpha,0}$ for each field component, and use a separate propagation equation for each. The total field is then the sum of these different components,

$$E=E_p+E_s+E_i=A_pe^{\imath\Xi_p}+A_se^{\imath\Xi_s}+A_i^*e^{-\imath\Xi_i}+\text{c.c.} \tag{18}$$

Because the wave equation, Eq. (1), is linear in the electric field, we can use Eq. (18) in the theory of Sec. II, then split the propagation equation into a separate GFEA-like equation for each field component in the usual way [3].

Our chosen nonlinear crystal is congruent $LiNbO_3$, for which we calculate refractive index and dispersion data from the Sellmeier equations of Jundt [14]. We model the nonlinear polarization using the square of the total electric field, retaining the parts resonant with our field carriers in the normal way. Our OPO simulations (see Sec. V) assumed a pump frequency of 357.1 THz, with nominal signal and idler carrier frequencies of 257.5 THz and 99.6 THz, respectively (wavelengths 0.84000 μm, 1.16500 μm, 3.0110 μm). This means that the pump pulse will travel through $LiNbO_3$ more slowly than the signal, and it therefore needs to be injected into the crystal ahead of it (see Fig. 1). When the two overlap, an idler is generated by the nonlinear interaction, and the three pulses then continue to interact with each other as they propagate through the crystal. Note that our ideal nondegenerate parametric amplifier simulations (see Sec. IV) use the same field frequencies, but idealize the crystal parameters by setting the group velocities and dispersions to zero.

A. System scalings

In a typical experiment, the crystal length would be fixed, as would any properties defined by its design, such as periodic poling. If we were to investigate this case for a range of

pulse durations, there would naturally be differences between the results, even within the SVEA. For example, the relative pulse broadening caused by traveling through a 1000 μm crystal is greater for a 12-fs pump pulse than for a 48 fs one. Similarly, a fixed timing offset for injection would have different effects; and a fixed pump pulse power would generate different strengths of nonlinear interaction for different pulse lengths. All these effects would confuse any attempt at a systematic comparison of the few-cycle effects in the models we consider.

Therefore, in order to isolate specific few-cycle effects, we must scale the pump pulse full width at half maximum (FWHM) $\mathcal{T}_p$, crystal length L_c, pump pulse energy $\mathcal{W}$, and pump timing offset t_Δ in such a way as to ensure the effects of group velocity, pump timing, and nonlinearity occur in the same proportions to one another over the range of pulse lengths.

We can work out an appropriate scaling by examining a simple version of the propagation equation (Eq. 11), where we write the group velocity prefactors as B_1, the second-order dispersion prefactors as B_2, and the polarization terms as CA^2. To assist us with the scaling process we also write $\xi = r^{-f}\xi'$, $\tau = r^{-g}\tau'$, and $A = r^h A'$, where r is the scaling factor. Our simple propagation equation is therefore

$$r^{h+f}\partial_{\xi'}A' = r^{h+g}B_1\partial_{\tau'}A' + r^{h+2g}B_2\partial^2_{\tau'}A' + r^{2h}CA'^2. \tag{19}$$

We can easily match the LHS term with the polarization term by setting $f=h$; but then we must choose either $h=g$ to match group velocities, or $f=2g$ to match the second-order dispersion—we cannot match both. For our chosen OPO situation (see Sec. V), it is best to match the group velocity terms, which control how long the pump and signal pulses overlap—in general, the dispersion has a much smaller effect.

We take our reference situation to be a 20-nJ 24-fs FWHM pump pulse propagating through a 500 μm crystal, with a pump timing offset of 48 fs. For the chosen parameter scaling ($f=g=h$)

$$\frac{\mathcal{T}_p}{24\ \text{fs}} = \frac{L_c}{500\ \mu\text{m}} = \frac{t_\Delta}{48\ \text{fs}} = \frac{20\ \text{nJ}}{\mathcal{W}}. \tag{20}$$

We could choose to make the scaling perfect, by also scaling the crystal parameters. If we scale the crystal dispersion with $B_2 = r^{-g}B_2'$, the relative amount of pulse spreading changes to become the same for each simulation—e.g., if the 48 fs pulse widens by 10% in a 1000 μm crystal, the 12 fs will also be widen by 10% in its 250 μm crystal. We did a set of SVEA simulations on this basis, and as expected, saw identical pulse profiles regardless of the chosen pulse length. However, we chose not to use this perfect scheme for the bulk of our OPO simulations, because it is far from being experimentally practical.

IV. IDEAL PARAMETRIC INTERACTIONS

A parametric amplifier is a single-pass device: pump and signal pulses are injected into one end of the nonlinear crystal, they interact within it, then exit at the far end. However, because real nonlinear crystals (such as $LiNbO_3$) tend to have significant dispersion, very short pulses quickly spread out, making them difficult to create, and reducing the few-cycle effects we aim to study.

FIG. 2. NPA, nondegenerate parametric amplification. The thickness of the arrows is intended to give an indication of how the energy of the field components changes during propagation through the crystal.

In order to demonstrate clearly the nature of few-cycle effects in $\chi^{(2)}$ materials, in this section we investigate an ideal case by setting the dispersion to zero, and make the group velocity the same at all frequencies. This means that $\sigma=1$, so the ''few-cycle'' polarization prefactor $\mathcal{K}$ is identical for both the SEWA and GFEA theories. Note that it is difficult to do no-dispersion simulations over long times, because pulse self-steepening causes both the numerical integration and the theoretical approximations to break down.

We inject Gaussian pump and signal pulses at exactly the same time (i.e. $t_\Delta=0$), with the same width. They then travel down the crystal with maximum overlap, interacting all the way. Other parameters are fixed by the scaling rules from Sec. III A. Further, when *graphing* results for the figures, we scale the times for each pulse length to the 6 fs case (e.g., for a 24 fs pulse, ''$\tau=10$'' corresponds to 40 fs), and scale the pulse intensities in proportion to their initial intensities. This means that graphs of the initial conditions for a range of pulse lengths would be identical.

Finally, note that in these ideal results, the nonlinear interaction is ''strong,'' with significant transfer of energy between the fields.

A. Nondegenerate parametric amplification (NPA)

We consider first a nondegenerate parametric amplifier with pump, signal, and idler frequencies such that $\omega_p \to \omega_s + \omega_i$ and $\omega_s \neq \omega_i$. In the 24 fs reference case, the initial pump energy is 20 nJ and the initial signal energy is 10 pJ, with a negligible (but finite) idler. For other pulse durations, the energies were scaled according to Eq. (20). Figures 2 and 3 show how, according to the GFEA, the idler pulse intensity profiles $|A_i|^2$ generated in a single pass of the crystal vary with pulse duration. The profiles show little variation with pulse duration except for the shortest pulses ($\tau \lesssim 20$), where distortion is evident; the signal and pump profiles show deviations of a comparable magnitude. More dramatic effects appear in the phase profiles: in Fig. 4, the phases of the pulse envelopes at pulse durations of 18 fs and 96 fs are shown with the phase distortions due to the finite pulse lengths [see Eq. (13)]. As the pulse duration shortens, the principal effect is to increase the magnitude of the phase distortion, leaving the shape of each profile largely unchanged; however, more complex phase oscillations develop for the shortest pulses. At 96 fs, the profiles show a smaller distortion, and are tend-

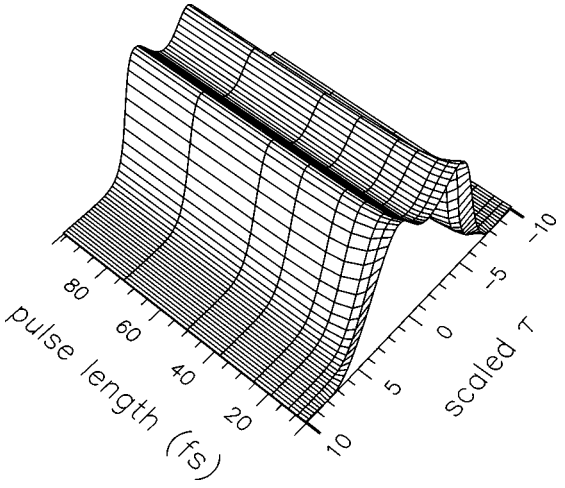

FIG. 3. NPA, scaled GFEA idler pulse envelopes $|A|^2$ on exit from the ideal dispersionless crystal. The SVEA results for *all* pulse lengths are essentially identical to the 96 fs result.

ing towards the long-pulse SVEA limit. In this limit, the profiles are essentially flat, although the pump field develops nodes that give rise to a steplike change in the phase.

B. Nondegenerate parametric deamplification (NPD)

As a variant on the case just treated, signal and idler pulses with equal numbers of photons were injected, and the relative phases of the pulses set to ensure that the signal and idler experience initial deamplification (see Fig. 5). Since the subsequent evolution is sensitive to phase changes, and the finite pulse length terms in the GFEA affect the phases, this is an interesting situation to examine. In the SVEA, the signal and idler decay away towards zero as the pulses propagate, so the SVEA output signal is just some residual part of the input. The GFEA evolution is different, as can be seen from Eq. (13)—the finite pulse lengths alter the phase profile of the nonlinearity, and hence change the evolution of the pulses. During an initial period of deamplification, the pulses undergo a gradual phase distortion. Then, as the discrepancy

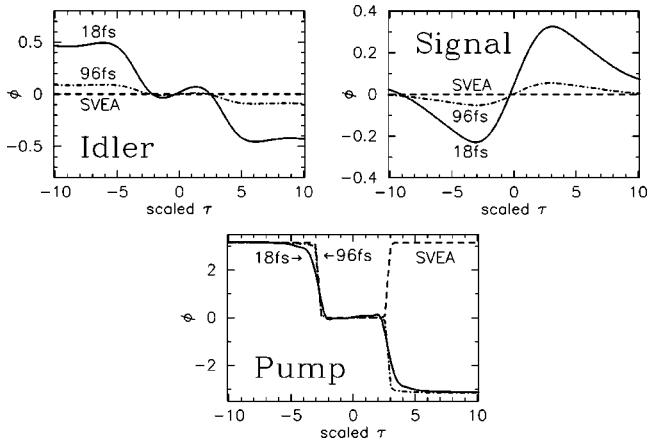

FIG. 4. NPA, envelope-phase profiles for 18- and 96-fs pulse durations. Top to bottom, idler, signal, pump; SVEA (dashed line), GFEA 96 fs (dash-dotted line), GFEA 18 fs (curved line).

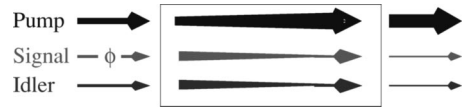

FIG. 5. NPD, nondegenerate parametric deamplification. The thickness of the arrows is intended to give an indication of how the energy of the field components changes during propagation through the crystal.

increases, amplification takes over. In a comparison of SVEA and GFEA models, the effect caused by the phase distortion is more visible when the interaction is strong enough for the input component of the signal pulse to be strongly depleted, and also is much stronger for shorter pulses

The GFEA signal pulse profiles on exit from the crystal as a function of pulse duration are presented in Fig. 6. Note that the SVEA prediction corresponds to the long-pulse limit of the GFEA figure, but those limiting features are too small to be seen. The GFEA output pulse energies are displayed in Fig. 7, which shows how the behavior changes both with pulse length and initial phase. The data for $\phi_{\text{signal}}=\pi/2$ demonstrates the effects of exact initial conditions and finite pulse length; maximum deamplification occurs in the long-pulse (SVEA) limit. If we instead start with a signal phase slightly different from $\pi/2$, e.g., 0.51π, the deamplification is less efficient and will eventually be overtaken by the amplification, even for the SVEA model. Consequently, comparisons for imperfect initial phases are dependent on the length of the crystal. However, since we use a scaling procedure, the results still behave in a systematic way, even if they are not completely generic.

Of course, changing other initial conditions can also disturb the deamplification, e.g., different numbers of signal and idler photons. Although both signal and idler will initially be deamplified, as they approach zero photon number, one field will ''overshoot'' the zero and be inverted. This alters the phase relationships, and so again amplification takes over. As an example, simulations based on our 18 fs pulses suggested

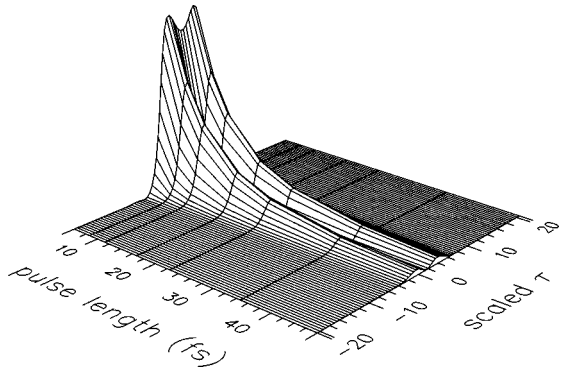

FIG. 6. NPD, output GFEA signal intensities for $\phi_s=\pi/4$ and $\phi_p=0$ for a range of pulse durations, peak value $\approx 6\times 10^5$. Equivalent SVEA results are very different, they are the same for all pulse lengths, are too small to show up on the scale of this graph (being $\sim 3\%$ of the height of the 48-fs GFEA peaks), and the two peaks are located further from the origin (at $\tau\approx\pm 10$).

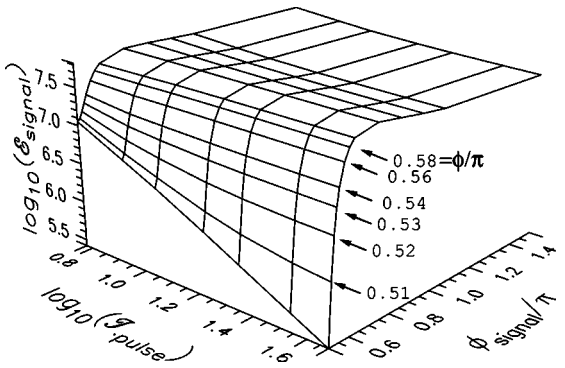

FIG. 7. NPD, output GFEA pulse energies ($\mathcal{E}_{\text{signal}} = \int |A_{\text{signal}}|^2 d\tau$, arbitrary units) for a range of initial signal (envelope) phases ϕ_s and pulse lengths $\mathcal{T}_{\text{pulse}}$. The intensities and times are scaled in our usual way. The SVEA results are nearly identical for all pulse lengths, and differ from the 48 fs [i.e., $\log_{10}(48) = 1.68$] results in that the near $\phi_{\text{signal}} = \pi/2$ give significantly lower energies—down to 10^4 rather than 3×10^5 for $\pi/2$.

that photon number mismatches of about 1% would not noticeably disrupt the appearance of either Fig. 6 or 7.

V. OPTICAL PARAMETRIC OSCILLATION (OPO)

We move on from optical parametric amplification to a synchronously pumped optical parametric oscillator (OPO). As shown in Fig. 8, we considered the case of a $LiNbO_3$ crystal in an optical cavity with mirrors that reflect the signal wavelength only. The oscillator is driven by a train of Gaussian pump pulses whose periodicity closely matches the natural period of the cavity, and which amplify, and then sustain the signal pulse confined within it. The cavity length can be ''tuned'' about exact synchronization. The idler pulse, generated when the signal pulse interacts with each new pump pulse, is transmitted through the output mirror with the pump, while the signal is strongly reflected. For a given set of parameter values, we modeled the development of the signal pulse over many cavity transits until it reached a steady state. Typically, we found that the signal stabilized in several hundred transits although, in a few cases, no equilibrium was achieved and the system oscillated indefinitely. Here we present results for the perfectly phase matched, sychronized case.

A. Scaled OPO

The complex nature of the dynamics, which arises from repetitive cycling of the signal pulse in the presence of many interacting processes makes the isolation and analysis of few-cycle effects within the different models quite compli-

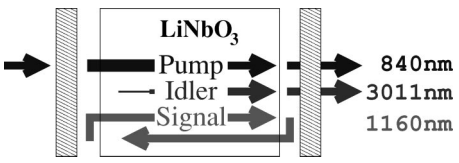

FIG. 8. Simplifed optical parametric oscillator experiment setup (see Sec. V).

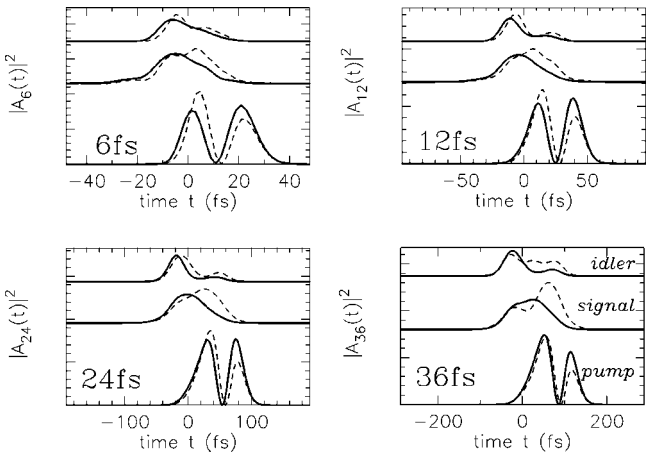

FIG. 9. Scaled OPO, time domain representation of the modulus squared of the pulse envelopes, for a range of injected pump pulse durations: 6 fs (top), 12, 24, 36 fs (bottom). For each subfigure, the curves compare (bottom to top) pump, signal, and idler for the SVEA simulations (dashed) and GFEA ones (curved).

cated. Figure 9 shows intensity profiles for the pump, signal, and idler (bottom to top in each frame) for the SVEA (dashed line) and GFEA (solid line) for four different pulse durations.

The first point to note in Fig. 9 is that the SVEA results are not identical in all frames, even though the scaling procedure in Sec. III A is designed to make them, as far as possible, *independent* of pulse duration. The reason is that the dispersion scales in a different way to the group time delay, and so is not correctly compensated by Eq. (20). A second rather surprising feature is that we might expect the GFEA results to tend to the SVEA as pulse length increases, but this is not evident from the graphs. The explanation for this is that the steady state of the OPO can change suddenly as the parameters are varied. This property is highlighted in Fig. 10, which shows the GFEA signal pulse profile for pulse durations from 6 fs to 192 fs; the sudden adjustment of the GFEA when moving from 36 fs to 48 fs takes it close to the SVEA, and the difference between the two gradually disappears as the pulse duration is increased further (see Fig. 11 and Ref. [11]). Note that the scaling procedure used for Fig. 10 is an extension of Eq. (20) in that the dispersion term is also scaled, making the SVEA results completely independent of pulse duration. Spectral profiles corresponding to the temporal profiles of Fig. 9 are shown in Fig. 12. The spectral shape for each field is similar across all pulse durations, with a pulse of double the (time) width naturally having half the bandwidth. Notice that the pump and signal spectra in the 6 fs frame are close to overlapping, which indicates that the separation of the total field into distinct pump, signal, and idler components is becoming a questionable assumption. Inclusion of the carrier wave in the results raises some quite subtle issues that need careful consideration. It must be stressed again that the carrier drops out of the analysis leading to Eq. (11). The envelope description is therefore complete, although the phases of two of the three envelope functions can be changed by arbitrary constants without any effect on the computations apart from an appropriate adjustment in the phase of the third envelope. For instance, if the

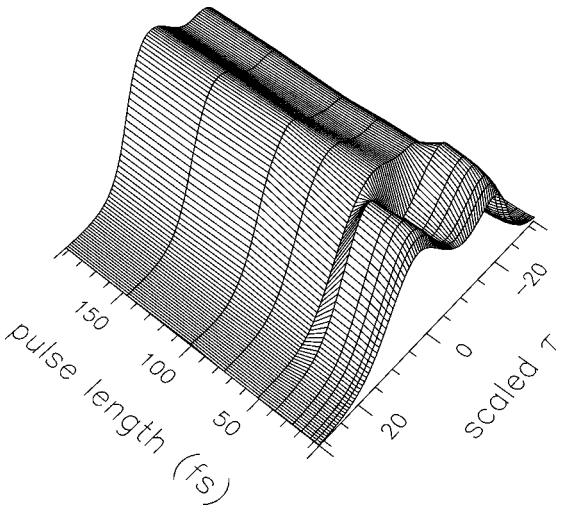

FIG. 10. Dispersion scaled OPO, time domain representation of the GFEA signal amplitude, for a range injected pump pulse durations from 6–192 fs. Here the crystal dispersion is adjusted in addition to the other scalings to make a SVEA theory fully scale invariant. The SVEA profile in this case very similar to the 192-fs GFEA profile.

phases of the pump and signal envelopes are changed by $\Delta\phi_p$ and $\Delta\phi_s$, the phase of the idler envelope is changed by $\Delta\phi_i=\Delta\phi_p-\Delta\phi_s$. Adjustments of this kind show up in the results only if graphs of the complete electric-field profiles, including the carrier waves, are displayed, as in Fig. 13. If the simulations in that figure were rerun with differing envelope phases, this would be reflected in temporal displacements of the carrierlike oscillations beneath the envelopes.

A further interesting feature is that, while the moduli of the pulse envelopes may have stabilized in a simulation, the envelope phases can (and usually do) change from pass to pass; this process continues indefinitely, so a movie made up of frames from successive transits would show the pump, signal, and idler electric-field oscillations drifting across underneath the respective steady envelope profiles. The different models discussed in this paper give significantly different results for the pass-to-pass phase drift. Figure 14 shows the phase change for the signal pulses as a function of pulse length for the SVEA, SEWA, and GFEA; note that the SEWA and GFEA results are similar to each other, while the (less accurate) SVEA exhibits a very different dependence.

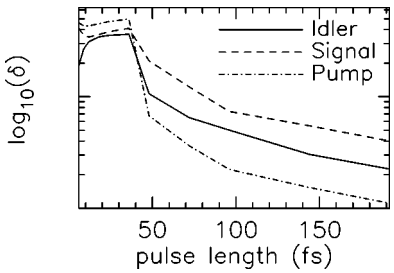

FIG. 11. Dispersion scaled OPO, maximum difference between GFEA and SVEA simulations over the middle quarter of the scaled τ range, on a $\log_{10}$ scale.

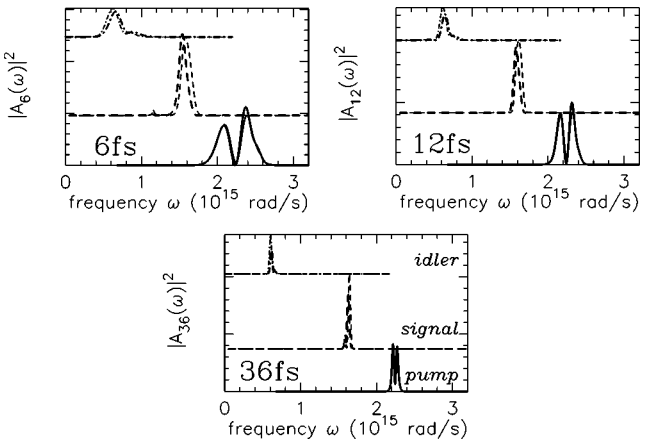

FIG. 12. Scaled OPO, frequency domain representation of the modulus squared of the pulse envelopes, for pump pulse durations of 6, 12, and 36 fs. For each subfigure, the curves compare (bottom to top) pump, signal, and idler for the SVEA simulations (dashed line) and GFEA ones (curved line).

The reference point used in calculating the phase drift is at the maximum amplitude of the envelope of the signal pulse, which is in fact not necessarily at the point of maximum electric field. This is a good choice for our purposes, because it does not move between passes once a steady state is established. Although these phase drifts are quite small, discrepancies between the SVEA and GFEA will quickly accumulate.

VI. CONCLUSIONS

We have presented a different and more complete derivation of how the envelopes of extremely short optical pulses evolve in nonlinear interactions. We have compared the results of our new (GFEA) model to those of the traditional slowly varying envelope approximation (SVEA) using a

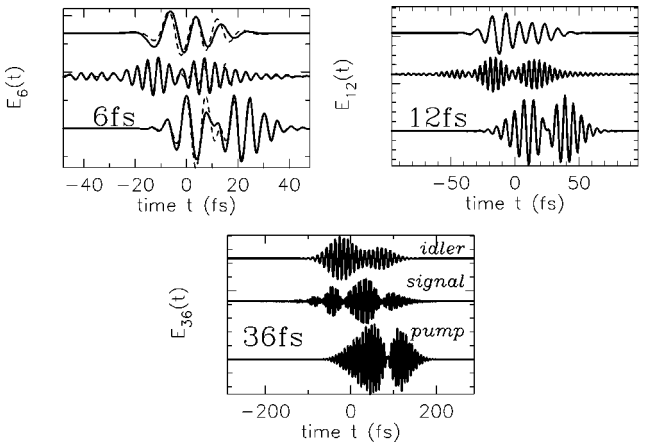

FIG. 13. Scaled OPO, time domain representation of the electric fields of the pulse, for pump pulse durations of 6, 12, and 36 fs. For each subfigure, the solid curves (curved line) compare (bottom to top) pump, signal, and idler for the GFEA simulations, for 6 fs the SVEA fields are also indicated (dashed line). The phases are chosen so that the maximum excursion of the signal envelope is purely real valued, and the idler phase is chosen so that $\phi_s+\phi_i=\phi_p$.

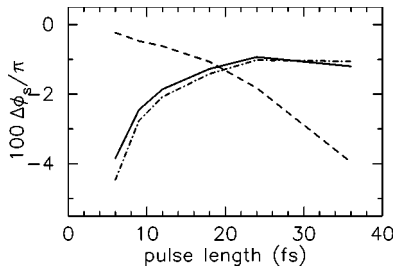

FIG. 14. Scaled OPO, pass-to-pass phase drift for a range of parameters, comparing SVEA (dashed line), GFEA (curved line), and SEWA (dash dotted line) simulation results. The differences are taken between the phase at the peak of the modulus-squared of the envelopes at the end of one pass of the signal pulse and the next.

scaling procedure to distinguish specific few-cycle effects from other phenomena caused by changing pulse duration. It should be noted that the SVEA becomes inadequate, whenever the envelope changes rapidly within a few carrier periods. Strictly speaking, a few-cycle pulse is not required, because a steep edge within a longer pulse also fulfills the conditions.

The effect of the extra ''few-cycle'' terms in the GFEA evolution equation is to add a phase distortion to the nonlinear polarization term, which then imposes itself on the pulse envelopes. This is demonstrated by our single-pass optical parametric amplifier NPA model where, whilst the SVEA model is insensitive to pulse length, the GFEA theory shows clear changes as the pulses get shorter and contain fewer optical cycles.

Further, when we studied the highly sensitive deamplification case (i.e. NPD), we saw dramatic differences between the SVEA and GFEA simulations even outside the few-cycle regime. These arose from the phase distorting effects of the few-cycle terms in the theory disrupting the exact phase relationships needed for deamplification. While the absolute size of these differences do depend on the chosen parameters of crystal length, pulse energy, and so on, they will always get dramatically larger for shorter pulses.

On the other hand, the repetitive cycling nature of the optical parametric oscillator (OPO) produces more complicated and subtle dynamics; small changes in parameter values can, for instance, cause sudden changes in the steady-state fields. It is therefore no surprise that comparison of the results predicted by the different models is less straightforward in the OPO case. The new model certainly produces differences in the pulse envelopes as well as the phases, although the way in which the GFEA tends to the SVEA in the long-pulse limit has some interesting features. The two models also predict different results for the pass-to-pass phase drift of OPO pulses, and this implies significant differences in the electric-field structures. In both cases, the carrier wave moves under the envelope from one transit to the next, but by different amounts.

[1] T. Brabec and F. Krausz, Phys. Rev. Lett. **78**, 3282 (1997).
[2] M.A. Porras, Phys. Rev. A **60**, 5069 (1999).
[3] Y.R. Shen, *Principles of Nonlinear Optics* (Wiley, New York, 1984).
[4] A.V. Tarasishin, S.A. Magnitskii, and A.M. Zheltikov, Opt. Commun. **193**, 187 (2001).
[5] T. Beddard, M. Ebrahimzadeh, D.T. Reid, and W. Sibbett, Opt. Lett. **25**, 1052 (2000).
[6] A. Baltuska, Z. Wei, S. Pshenichnikov, and D. Wiersma, Opt. Lett. **22**, 102 (1997).
[7] J.K. Ranka and A.L. Gaeta, Opt. Lett. **23**, 534 (1998).
[8] S. Tzortzakis, L. Sudrie, M. Franco, B. Prade, A. Mysyrowicz, A. Couairon, and L. Berge, Phys. Rev. Lett. **87**, 213902 (2001).
[9] N. Akozbek, M. Scalora, C.M. Bowden, and S.L. Chin, Opt. Commun. **191**, 353 (2001).
[10] A.L. Gaeta, Opt. Lett. **27**, 924 (2002).
[11] P. Kinsler and G.H.C. New, e-print arXiv.org/physics/0212016.
[12] S.M. Gallagher-Faeder and D.M. Jonas, Phys. Rev. A **62**, 033820 (2000).
[13] P. Kinsler, e-print arXiv.org/physics/0212014.
[14] D.H. Jundt, Opt. Lett. **22**, 1553 (1997).